An integrated approach to flood hazard assessment on alluvial fans using numerical modeling, field mapping, and remote sensing

Jon D. Pelletier[†]
Larry Mayer
Department of Geosciences, University of Arizona, 1040 E. Fourth Street, Tucson, Arizona 85721, USA

Philip A. Pearthree
Arizona Geological Survey, 416 W. Congress Street, Suite 100, Tucson, Arizona 85701, USA

P. Kyle House
Nevada Bureau of Mines and Geology, Mail Stop 178, University of Nevada, Reno, Nevada 89557, USA

Karen A. Demsey
3055 NE Everett Street, Portland, Oregon 97232, USA

Jeanne E. Klawon
U.S. Bureau of Reclamation, P.O. Box 25007, Denver, Colorado 80225, USA

Kirk R. Vincent
U.S. Geological Survey, 3215 Marine Street, Boulder, Colorado 80303, USA

ABSTRACT

Millions of people in the western United States live near the dynamic, distributary channel networks of alluvial fans where flood behavior is complex and poorly constrained. Here we test a new comprehensive approach to alluvial-fan flood hazard assessment that uses four complementary methods: two-dimensional raster-based hydraulic modeling, satellite-image change detection, field-based mapping of recent flood inundation, and surficial geologic mapping. Each of these methods provides spatial detail lacking in the standard method and each provides critical information for a comprehensive assessment.

Our numerical model simultaneously solves the continuity equation and Manning's equation (Chow, 1959) using an implicit numerical method. It provides a robust numerical tool for predicting flood flows using the large, high-resolution Digital Elevation Models (DEMs) necessary to resolve the numerous small channels on the typical alluvial fan. Inundation extents and flow depths of historic floods can be reconstructed with the numerical model and validated against field- and satellite-based flood maps. A probabilistic flood hazard map can also be constructed by modeling multiple flood events with a range of specified discharges. This map can be used in conjunction with a surficial geologic map to further refine floodplain delineation on fans.

To test the accuracy of the numerical model, we compared model predictions of flood inundation and flow depths against field- and satellite-based flood maps for two recent extreme events on the southern Tortolita and Harquahala piedmonts in Arizona. Model predictions match the field- and satellite-based maps closely. Probabilistic flood hazard maps based on the 10 yr, 100 yr, and maximum floods were also constructed for the study areas using stream gage records and paleoflood deposits. The resulting maps predict spatially complex flood hazards that strongly reflect small-scale topography and are consistent with surficial geology. In contrast, FEMA Flood Insurance Rate Maps (FIRMs) based on the FAN model predict uniformly high flood risk across the study areas without regard for small-scale topography and surficial geology.

Keywords: flood hazard, alluvial fan, surficial geology, remote sensing, numerical modeling.

INTRODUCTION

Alluvial fans may be divided into two process-based types: debris flow fans and streamflow fans, with important implications for flood hazards. Debris-flow fans are often more geomorphically unstable than streamflow fans because their debris fills channels and triggers more frequent avulsions (National Research Council, 1996). Debris flows have a relatively high viscosity, however, leading to localized flood risk on steep, proximal fan areas. Low-relief fans of both types, however, can exhibit rapid channel changes that should be incorporated into flood hazard assessments.

The goal of this study is to integrate four assessment methods on two low-relief streamflow fans in southern and central Arizona (location map in Fig. 1). These areas were chosen based on their historical flood complexity. Both fans have unusually low relief that results in complex flow patterns and rapid (decadal-scale) channel changes. For example, only decimeters of relief separate areas of active flooding from areas that have not received flooding for thousands of years or longer on these fans. In addition, the Tortolita and Harquahala piedmonts have unusually complete hydrologic and geomorphic databases, including high-resolution DEMs, 1:24,000-scale surficial geologic maps, paleoflood records, and detailed inundation maps for recent extreme floods. Both fans are streamflow fans, not debris-flow fans, because of the relatively low relief and minimal regolith cover of their upstream drainage basins and the distance (i.e.,

[†]E-mail: jon@geo.arizona.edu.

GSA Bulletin; September/October 2005; v. 117; no. 9/10; p. 1167–1180; doi: 10.1130/B255440.1; 12 figures; 1 table.

several kilometers) that separates the mountain front from their distributary zones.

The spatial occurrence of modern fan flood hazards is often controlled by the late Cenozoic fan evolution. Many alluvial fans in the western United States, for example, exhibit a suite of terraces that rises up from the active channel like a flight of stairs. These terraces may be formed by climatically driven sediment pulses from the upstream drainage basin (e.g., Reheis et al., 1996; Bull, 1991), from tectonic uplift (Hooke, 1972; Rockwell et al., 1985), or from the internal dynamics of the fluvial system (Ritter, 1967; Schumm and Parker, 1973). In the simplest case, the active channel is flanked by pairs of terraces that increase in age with distance from the modern channel (Fig. 2A). These older terraces are generally not subject to flood inundation, especially in the proximal area of the fan where relief between terraces and the active channel is greatest. The geomorphic evolution and surficial geology of most fans is more complex than the simple case shown in Figure 2A, however. On the southern Tortolita piedmont, for example, terraces of variable age interfinger to produce a complex map geometry. Nevertheless, the active portion of the proximal fan area is confined to a narrow region, flanked by older deposits, that widens out in the distal fan area.

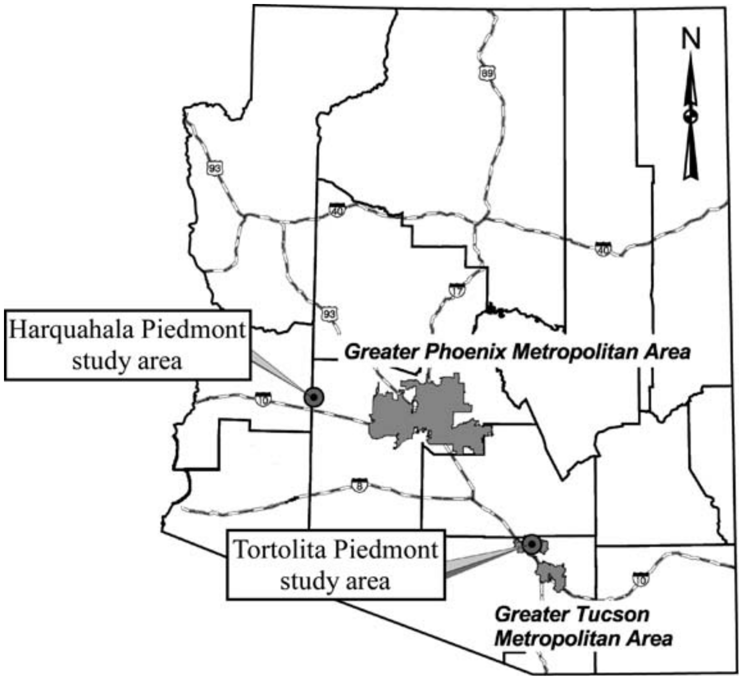

Figure 1. Study site location map.

The combination of complex flow conditions and minimal topographic relief renders many standard flood routing methods inapplicable on alluvial fans. The step-backwater method, for example, which successively calculates water-surface elevations along a profile using the energy equation, can usually be applied only when flow is constrained at downstream cross sections. This requires that flow paths be known a priori. In addition, the step-backwater method is limited to one-dimensional (centerline-parallel) flows. On active fans, flow concentrated near the apex is distributed between many downstream channels and adjacent overbank areas, rendering flow depths and velocities very difficult to model throughout the system.

The delineation of flood-prone areas using the FAN model (Dawdy, 1979; FEMA, 1990) is an alternative to hydraulic modeling, but the FAN model makes a number of simplifying assumptions and does not include small-scale topography or surficial geology in a significant way. In its simplest form, the FAN model treats alluvial fans as cone segments with a uniform probability of flooding in each direction within the "active" portion of the fan. Flood risk at any particular location is a function only of the estimated peak discharge at the fan apex and the fan width at that location. The predictions of the FAN model are particularly sensitive to how the active portion of the fan is defined. The active fan has often been defined as areas with distributary drainage (FEMA, 2000), but field observations indicate that older deposits with tributary drainage can be flooded near their margins. Conversely, surficial geologic mapping indicates that many areas with distributary drainage have not been subjected to deep flooding for thousands of years or longer.

The southern Tortolita piedmont (Fig. 3) is a dramatic example of the conservative nature of many FEMA floodplain maps based on the FAN model. The surficial geologic map for this piedmont (Fig. 3A) was constructed by integrating soil development and other indicators of surface age to group fan terraces into age ranges (McFadden et al., 1989). The surface age represents the approximate time since deep flooding occurred because soils would be stripped from a surface subjected to scour and buried on a surface subjected to significant fluvial deposition (although older deposits may be reworked at their margins during high flows). The FEMA map (Fig. 3B) identifies most of the southern Tortolita piedmont as within the regulatory floodplain. Very old (mid-Pleistocene) terraces on the upper fan areas, characterized by their high relief above the active channel, ridge-and-ravine topography, and tributary drainage, are correctly mapped as having no flood risk in the FEMA map. Most of the remaining areas, however, are mapped as part of the 100 yr floodplain. Surficial geologic mapping, in contrast, indicates that many of these surfaces are late Pleistocene or early Holocene in age. These older surfaces have not been subjected to significant flooding within the last 5000–100,000 yr based on their soil development. Therefore, the FEMA map overpredicts the probability of flooding by two to three *orders of magnitude* in some areas. The Tortolita piedmont is not unique in this regard; surficial geologic mapping has been used in alluvial-fan flood hazard assessments for several decades, and the resulting maps often contradict FEMA maps (e.g., Cain and Beatty, 1968; Field and Pearthree, 1991a; Pearthree et al., 1992; Pearthree et al., 2000; House, 2003).

Based on these discrepancies, the validity of the FAN model for defining flood hazards has been questioned by numerous experts (Fuller, 1990; Field and Pearthree, 1991b; House et al., 1991; Pearthree, 1991; Pearthree et al., 1992; French et al., 1993; Hjalmarson, 1994; National Research Council, 1996). FEMA recently revised its procedures to address these concerns (FEMA, 2000). This revised procedure specifically includes the identification of active and inactive portions of the fan using historical records and photographs as well as engineering and geomorphic evidence. As a result of these guideline changes, geomorphic evidence may now play an important role in official flood hazard assessments. Surficial geologic mapping in particular is a powerful method that provides a long-term assessment of flood-prone areas. This method does not apply directly to individual flood events, however, and

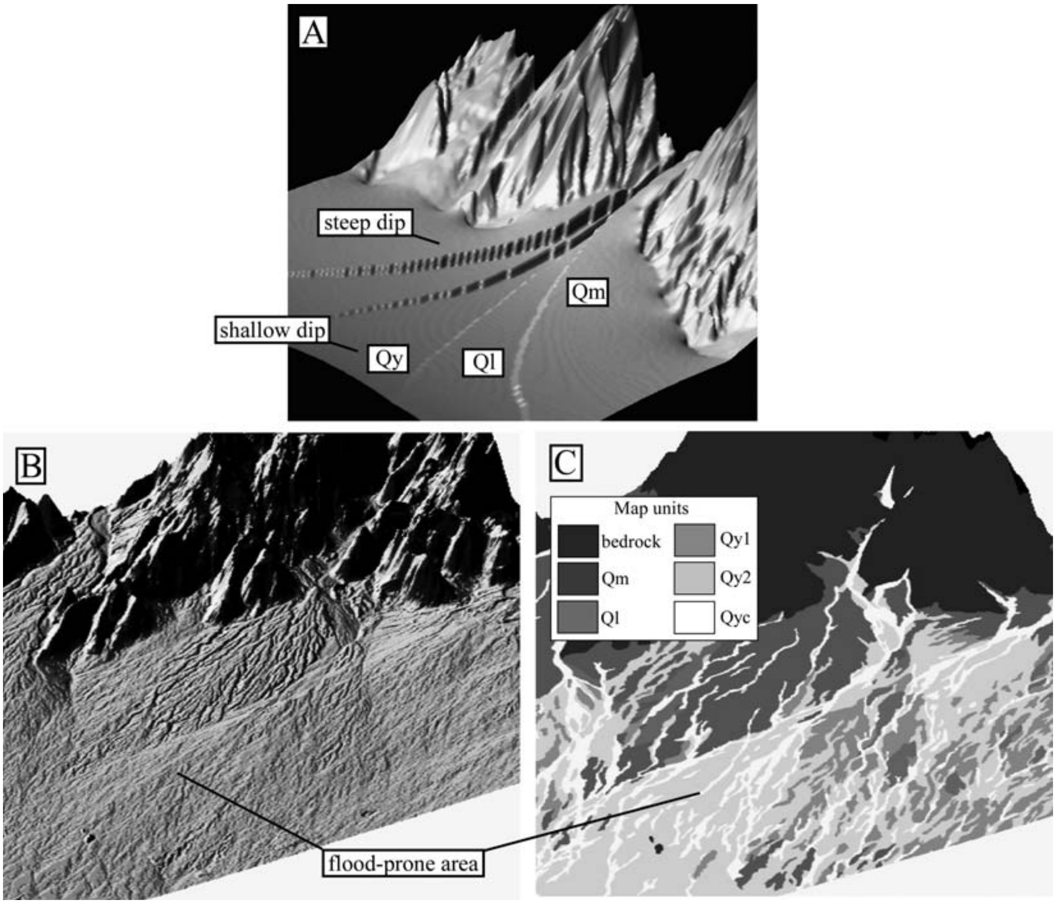

Figure 2. Influence of late Cenozoic geomorphic evolution on the spatial occurrence of modern flood hazards on fans. (A) Idealized fan geometry with an active channel and young deposits (Qy) flanked by pairs of terraces of increasing age (Ql—late Pleistocene; Qm—mid-Pleistocene) with distance from the active channel. Flooding is topographically confined to areas of Qy deposits. Oblique perspective of (B) topography (shaded relief of DEM obtained from Pima Association of Governments [PAG], 2000) and (C) surficial geology of the southern Tortolita piedmont (after Demsey et al., 1993; older fan deposits have darker shading). Flood hazards are concentrated in a narrow zone in the proximal fan area, widening out toward the distal portion of the fan, as in (A).

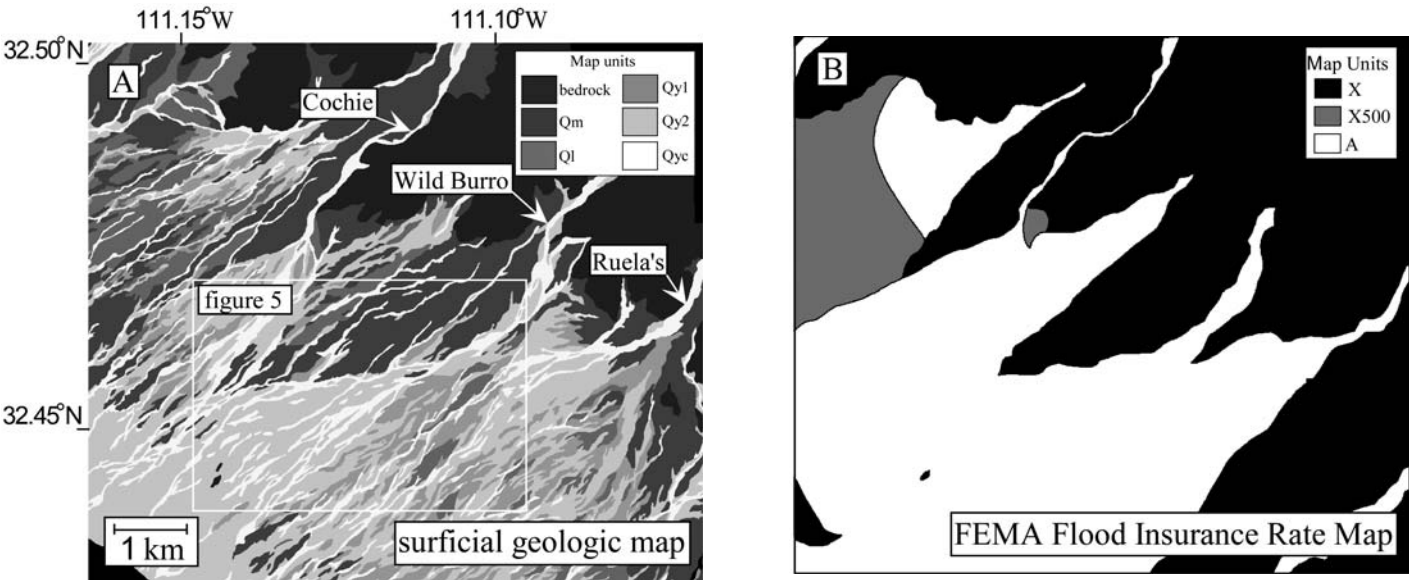

Figure 3. Southern Tortolita study area. (A) Surficial geology after Demsey et al. (1993). Approximate surface ages are Qm >100 ka, Ql = 100–20 ka, Qy1 = 20–5 ka, Qy2 <5 ka, and Qyc <5 ka. Units are the same as in Figure 2C. The locations of Cochie, Wild Burro, and Ruela's Washes are shown. (B) FEMA Flood Insurance Rate Map (after FEMA, 1999). X—outside 500 yr floodplain, X500—100–500 yr floodplain, A—100 yr (regulatory) floodplain.

it is not clear how surficial geologic maps relate to the standard regulatory flood. A new analytical method is needed to complement surficial geologic mapping by providing predictions for flood inundation and flow depths for a range of specified flood discharges. Numerical modeling can provide this analytical tool, and many two-dimensional flow models are currently available for use. The complexity of alluvial fans, however, demands a computationally efficient numerical model capable of handling the large, high-resolution DEMs that are needed to resolve the numerous small channels distributed across the typical alluvial fan.

A TWO-DIMENSIONAL RASTER-BASED HYDRAULIC MODEL FOR ALLUVIAL-FAN FLOODING

Alluvial fan flows are clearly two dimensional, so none of the classic one-dimensional (1D) hydraulic models such as HEC-2 is applicable. Many two-dimensional (2D) finite-element models have been developed in recent years, including RMA2 (King and Norton, 1978; U.S. Army Corps of Engineers Waterways Experiment Station, 2001), TELEMAC-2D (Galland et al., 1991), and FLO-2D (O'Brien et al., 1993), among others. These models solve the complete 2D St. Venant equations with turbulent closure. They have the advantage of modeling flows in much of their true complexity, but they are computationally intensive for even modest grid resolutions. As such, 2D finite-element models may not be the ideal approach for alluvial-fan flood modeling, where grids with more than a million pixels may be required to adequately resolve the numerous small channels distributed on the fan.

We developed a 2D raster-based numerical model that solves the continuity equation and Manning's equation simultaneously using an implicit numerical method. The equations and solution method are similar to two recently published models, but our code was developed independently. Using a high-resolution DEM as input, Bates and De Roo (2000) developed LISFLOOD-FP, which couples a 1D unsteady hydraulic model for flow in a main channel to a 2D raster-based model for overbank inundation of the adjacent floodplain. Our model essentially applies the floodplain component of LISFLOOD-FP to the fan as a whole. In testing, LISFLOOD-FP was found to predict extents of flood inundation comparable to finite-element methods (Bates and De Roo, 2000; Horritt and Bates, 2001a, 2001b, 2002). The dynamics of the flood wave, however, were not as accurately modeled with LISFLOOD-FP as with finite-element methods. This may not be a significant limitation for alluvial-fan flooding, however, because accurate predictions of flood dynamics are not as important as accurate predictions of flood inundation. Our model is also similar to Miyamoto et al. (2003), who applied the continuity equation and Manning's equation to simulating catastrophic outburst flooding on Mars. Notably, Miyamoto et al. (2003) also validated their model against analytic solutions for 2D flow on planes and in simple channels, providing further support for this computationally efficient approach.

The continuity equation is the basis for all flood-routing models and states that any imbalance in the discharge into and out of a pixel results in a raising or lowering of the flow depth within that pixel. In two dimensions, the continuity equation for unsteady flow is expressed as

$$\frac{dh_{i,j}}{dt} = \frac{Q_{x_{i-1,j}} - Q_{x_{i,j}} + Q_{y_{i,j-1}} - Q_{y_{i,j}}}{\Delta x \Delta y}, \qquad (1)$$

where $h_{i,j}$ is the flow depth at pixel (i,j), $Q_{x\,i,j}$ and $Q_{y\,i,j}$ are the discharges in the x and y directions, Δx and Δy are the pixel dimensions, d indicates a derivative, and t is time. Ideally, the unsteady flow equation would be used for all fan-flood modeling because alluvial-fan floods are often of short duration (hours). Our model assumes steady flow, however, for two practical reasons. First, very few channels on alluvial fans are gaged, so direct constraints on the duration of flooding are usually unavailable. Second, regulators specify the peak discharge of their design event (i.e., the 100 yr flood) but do not specify the hydrograph shape of that event. For our approach to be widely applicable, therefore, we cannot require that the hydrograph shape be known. With the time-dependent term removed, the continuity equation for steady flow is

$$\frac{Q_{x_{i-1,j}} - Q_{x_{i,j}} + Q_{y_{i,j-1}} - Q_{y_{i,j}}}{\Delta x \Delta y} = 0. \qquad (2)$$

Using equation 2 instead of equation 1 simplifies the analysis in two ways. First, only the peak flood stage needs to be specified, not the entire hydrograph. Second, each flood stage is associated with a unique flood inundation.

The continuity equation must be combined with a flow equation that relates the discharges in each pixel to the flow depths in order to obtain a single equation for flow depths. Our model uses Manning's equation as do many flow models. Manning's equation gives

$$Q_{x_{i,j}} = \frac{h_{i,j}^{5/3}}{n_{i,j}} \left(\frac{h_{i-1,j} - h_{i,j} + z_{i-1,j} - z_{i,j}}{\Delta x} \right)^{1/2} \Delta y, \qquad (3)$$

where $n_{i,j}$ is the roughness coefficient and $z_{i,j}$ is the bed elevation at pixel (i,j). Hydraulic radius is assumed to be closely approximated by flow depth, hence the $h^{5/3}$ term. The expression inside the parenthesis of equation 3 is the two-dimensional form of the water surface slope inside a pixel, thus we correctly use water surface slope to drive the flow.

Although overbank areas are clearly rougher than incised channels on most alluvial fans, we did not quantify this difference for the results of this paper. Our results indicate, however, that the assumption of uniform roughness does not preclude accurate results from being obtained for our study areas. In these areas, the distribution of incised channels on the fan appears to play the dominant role in determining the distribution of flooding by creating accommodation space for flow on the fan. The uniform-roughness assumption is not likely to be a reasonable approximation for all fans, however, and roughness values should be used if they are available for the study area. The assumption of uniform roughness further simplifies the analysis because n cancels out of the model equation (equation 3 input into equation 2) entirely. Similarly, since we used a DEM with square pixels, Δx and Δy also cancel out of the equation, and the model equation is a function of $h_{i,j}$ and $z_{i,j}$ only.

Equations 2 and 3 constitute a nonlinear boundary-value problem for the flow depths $h_{i,j}$ at each point of the grid in terms of the known bed elevations $z_{i,j}$. The flow depths at a cross section upstream from the study area are the only additional inputs required to solve the model. The input flow depths may be constrained in several ways depending on the available data. If the model is being used to reconstruct a historic flood and stream gage data is available near the apex, the flood stage can be directly used to constrain the flow depths at the stream gage cross section. To do this, the flood stage is added to the channel-bed elevation at the deepest point in the cross section to estimate the water-surface elevation. The flow depths for all of the remaining pixels of the cross section are then estimated as the difference between the water-surface elevation and the bed elevation of those particular pixels. Paleostage indicators (slackwater deposits and high-water marks) can be used to determine flow depths in a similar way if stream gage data is not available. If only the peak discharge is known (e.g., regional frequency-discharge relationships provide no information on flood stage), the flood stage must be inferred from the discharge. This latter method involves assuming a value for n at the cross section, so it is best to work directly with flood stage or depth constraints if possible. The water-surface slope is assumed to be zero at all boundary grid points where water flows out of the grid. The numerical model does not require that the flow paths be known a priori in order to enforce this boundary condition.

Equations 2 and 3 are solved for the entire grid simultaneously using Newton's method. This method iteratively finds the root of a nonlinear system of equations from any starting point (Press et al., 1992). To use Newton's method, a residual vector is defined that goes to zero when the exact solution is obtained. This residual vector is obtained by rearranging equation 2 to obtain

$$\boldsymbol{R} = \frac{Q_{x_{i-1,j}} - Q_{x_{i,j}} + Q_{y_{i,j-1}} - Q_{y_{i,j}}}{\Delta x \Delta y}. \tag{4}$$

Newton's method iteratively estimates the vector of flow depths for the entire grid, $\boldsymbol{h}$, using

$$\left[\frac{\partial \boldsymbol{R}}{\partial \boldsymbol{h}}\right]_k \left(\boldsymbol{h}_{k+1} - \boldsymbol{h}_k\right) = -\boldsymbol{R}_k, \tag{5}$$

where $\boldsymbol{h}_k$ is the vector of flow depths at the present iteration, $\boldsymbol{h}_{k+1}$ is the vector of flow depths at the new iteration, and $\boldsymbol{R}$ is the residual vector (bold indicates that $\boldsymbol{R}$ is a vector). Equation 5 is solved implicitly in our model using the Alternating-Direction-Implicit (ADI) technique (Press et al., 1992). This technique quickly converges to the exact solution for $\boldsymbol{h}$ from any starting point. A grid with all zeros is the usual starting point.

As a steady-flow model with a number of simplifying assumptions, our model does not simulate flood attenuation. In an alluvial-fan flood, peak flow can decrease as it moves downstream for three reasons. First, flow volume, and thus peak discharge, diminishes as water infiltrates into the substrate. Our modeling approach could be modified to include infiltration (or runoff generated locally on the fan) by adding a constant term in equation 2 to reflect losses (or gains) within each pixel. We did not include an infiltration term in order to keep our solution appropriate for the general case, and the consequence is that the model should overpredict discharge and the extent of flooding in downstream reaches. Second, alluvial-fan flood flows often branch into numerous channels and pass into overbank areas, but some of these threads of flow eventually reconverge. Flow generally propagates more slowly where it is shallow, and thus flood waves end up out of phase at downstream points of reconvergence. Our assumption of steady flow (equation 2) essentially forces flow to be in phase at all points of reconvergence, and the consequence is that the model should overpredict discharge and the extent of flooding in downstream reaches. Third, the flood wave may spread or diffuse if the flow is subcritical. It is generally agreed, however, that this component of flood-wave dispersion is not significant for steep fans. In fact, observations indicate that near-critical conditions often occur in alluvial-fan floods (French, 1987), which act to maintain steep gradients in water depth without attenuation. The hydraulic geometry of steep channels generally (Grant, 1997) and those of hydraulically steep alluvial fans specifically (Vincent and Smith, 2001) appear to evolve to accommodate critical flow conditions.

RECONSTRUCTIONS OF TWO HISTORIC FLOODS USING FIELD MAPPING, REMOTE SENSING, AND NUMERICAL MODELING

Description of the Study Areas

The southern Harquahala piedmont is dominated by a single, large drainage: Tiger Wash (Fig. 4). Tiger Wash is fed by a 300 km² tributary system that drains part of the Harquahala and Big Horn mountains and a moderately dissected basin between them. Tiger Wash floods in response to both monsoonal storms and more extensive frontal and tropical storms (Pope et al., 1998; FCDMC, 2003). As Tiger Wash enters the low relief fan at the upstream boundary of the study area, it changes from a tributary system to a large (120 km²), downstream-branching distributary-drainage system. Local topographic relief across the system is generally less than 2 m. This low level of relief, in combination with high discharges, makes Tiger Wash susceptible to rapid channel changes and extensive overbank flooding (Klawon and Pearthree, 2000; Field, 2001) as illustrated by the widespread Holocene deposits in the surficial geologic map (Fig. 4B). Channel deposits diminish in extent and fine-grained deposits become very extensive downstream in the distributary system. These deposits indicate that sheetflooding between and downstream of channels is a very important component of large floods on Tiger Wash.

The southern Tortolita piedmont, in contrast, is fed by five principal canyons that range in size from 6 to 19 km². Our study area (Fig. 3) encompasses three of the five major Tortolita canyons, including Cochie, Wild Burro, and Ruelas. The Tortolita piedmont primarily floods

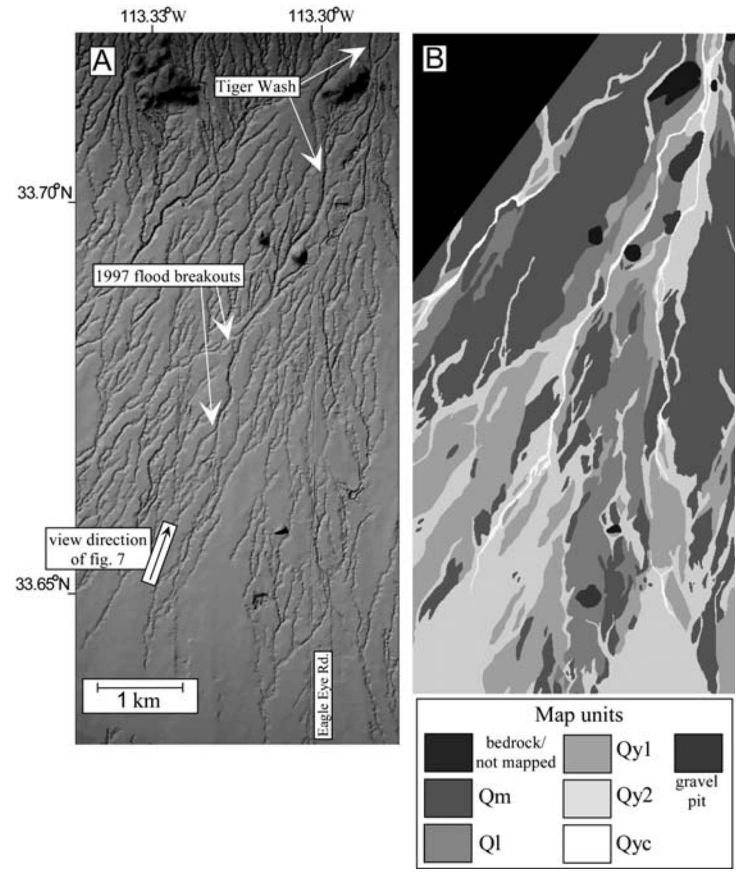

Figure 4. Southern Harquahala piedmont (Tiger Wash) study area. (A) Shaded-relief image of DEM (FCDMC, 2001). (B) Surficial geologic map (after Klawon and Pearthree, 2000). Surficial geologic units are equivalent to those of Figure 2.

in response to brief, monsoonal thunderstorms during the summer months (House, 1991). The Tortolita piedmont is predominantly characterized by incised channels that are separated by older fan deposits that have not experienced flooding for centuries or longer. In this section of the paper we focus primarily on Wild Burro Wash, the site of an extreme, well-documented flood in 1988.

Recent Flood Behavior and Frequency-Discharge Relationships for the Study Areas

The Tiger Wash drainage basin received between 100 and 300 mm of precipitation on 25 and 26 September 1997 as tropical storm Nora dissipated over western Arizona (FCDMC, 2003). Flooding occurred on the distributary portion of Tiger Wash on 26 September following the heaviest rains from Nora. The peak discharge of this event was inferred from high-water marks near the fan apex to be 260 m^3/s (J.E. Fuller Hydrology and Geomorphology, 2000). The stream gage record of Tiger Wash intermittently covers a 25 yr period from 1963 to the present. Using this record and the regional flood-envelope curve (Eychaner, 1984; Enzel et al., 1993), we estimated the 10 yr, 100 yr, and maximum flood discharges to be 100, 300, and 800 m^3/s, respectively (Table 1).

No stream gage data exist for any of the Tortolita canyons, so rainfall-runoff modeling, paleoflood indicators, and regional flood-envelope curves must be used. House (1991) performed paleoflood reconstructions for all five of the major Tortolita canyons using slackwater deposits and high-water marks in conjunction with HEC-2 modeling. He found that the largest paleoflood stage recorded in any of the Tortolita canyons had a discharge of 250 m^3/s near the fan apex. This extreme flood was concentrated in Wild Burro Canyon (Cochie and Ruelas canyons do not record paleoflood evidence for this event) and occurred on 27 July 1988. It is difficult to assign a recurrence interval to this event, but 100–1000 yr is an appropriate estimate based on the preservational time scales for slackwater deposits in this type of setting (House, 1991). Using the paleoflood record and the regional flood-envelope curve, we estimated the 10 yr, 100 yr, and maximum flood discharges to be 85, 250, and 350 m^3/s, respectively (Table 1).

Field and Satellite-Based Flood-Inundation Mapping of the Wild Burro Wash and Tiger Wash Floods

Field observations can be used to constrain inundation and flow regimes (e.g., deep channel flow, shallow sheetflooding) soon after a flood has occurred (e.g., Pearthree et al., 1992; Klawon and Pearthree, 2000; Youberg and Pearthree, 2002). Recent inundation is commonly indicated by undisturbed sediment ranging from coarse gravel to fine overbank and sheetflood deposits, organic flotsam, evidence of fresh scour, and the damage to intact vegetation. Areas of inundation during the 1988 flood in Wild Burro Wash (Fig. 5A) and the 1997 flood in Tiger Wash (Fig. 6A) were mapped in the field by Arizona Geological Survey teams in 1990 and 1999, respectively (House et al., 1992; Vincent et al., 2004; Pearthree et al., 2004). Flow in Wild Burro Wash was subdivided into four categories of flow based on depth (colors refer to those in Fig. 5A): between 0 and 10 cm (green), between 10 and 30 cm (orange), between 30 and 50 cm (red), and greater than 50 cm (maroon) using field indicators described in House et al. (1992) and Vincent et al. (2004). Flow in Tiger Wash was subdivided into three qualitative flow categories: channel flow, deep unconfined flow, and shallow unconfined flow (flow on the eastern branch of Tiger Wash was undivided, but was mostly comprised of shallow flow) based on criteria described in Pearthree et al. (2004).

Patterns of inundation associated with the Wild Burro and Tiger Wash floods show many similarities but also reveal some important differences. In both cases, flow in channels was responsible for the transport of bedload sediment up to small boulders and erosion of channel beds and stream banks. No substantial new channels formed during the Wild Burro flood, whereas two large channels ("breakouts") and several smaller channels formed during the Tiger Wash flood (Fig. 7). Relatively deep unconfined flow occurred in broad overbank areas adjacent to channels and downstream from them in both floods. This type of flow deposited gravel and sand sheets and streamlined pendant bars downstream from vegetation. Shallow (<30 cm) sheetflooding that occurred at the margins of flow and in broad sheets in the lower part of the distributary system was by far the most extensive category of inundation in both floods. Flow was distributed into multiple separate paths in each flood, but the distributary pattern was more complex and intricate in the Wild Burro flood.

As a complement to field-based geomorphic mapping, Mayer (2000) developed a satellite-based method using spectral changes between two Landsat images acquired immediately prior to and following a flood event. This technique enables a very large region (~10,000 km^2, or the area of a Landsat scene) to be rapidly assessed for changes that may reflect flood inundation. The change detection method requires that the two images be precisely coregistered and spectrally corrected so that changes can be determined on a pixel by pixel basis. Using bands 4 and 5, Mayer's method constructs an image with red, green, and blue channels representing decorrelation-stretched band 5 (after flood), band 4 (after flood), and band 5 (before flood), respectively. See Mayer (2000, 2002) for more details on the implementation of this method.

Mayer and Pearthree (2002) utilized the change detection method to map the inundation and associated surface changes of the 1997 flood in Tiger Wash. The yellow, cyan, and blue colors on the change image (Fig. 6B) highlight areas where landscape change occurred between July and October 1997. Relict Pleistocene surfaces and other fan areas that were not seriously affected by flooding are represented by shades of magenta. The yellow color represents areas

TABLE 1. DISCHARGE ESTIMATES USED FOR MODEL INPUTS

	Tiger Wash (m^3/s)	Wild Burro (m^3/s)
Input location (UTM 12S)	287520, 3733510	491120, 3592160
Drainage area (km^2)	300‡	11.1†
Recurrence Interval (yr)		
10	100#	85‡‡
100	300#	250†
Maximum	800‡	350††
Comparison data		
HEC-1 Q_{100}	600§	300†
FEMA Q_{100}	nd	270†
Maricopa/Pima Q_{100}	200#	280†

†House (1991).
‡CHM2Hill (1992) paleoflood results.
§CHM2Hill (1992) HEC-1 results.
#FCDMC (2002, personal commun.).
††Eychaner (1984).
‡‡Follows same ratios as Tiger Wash.

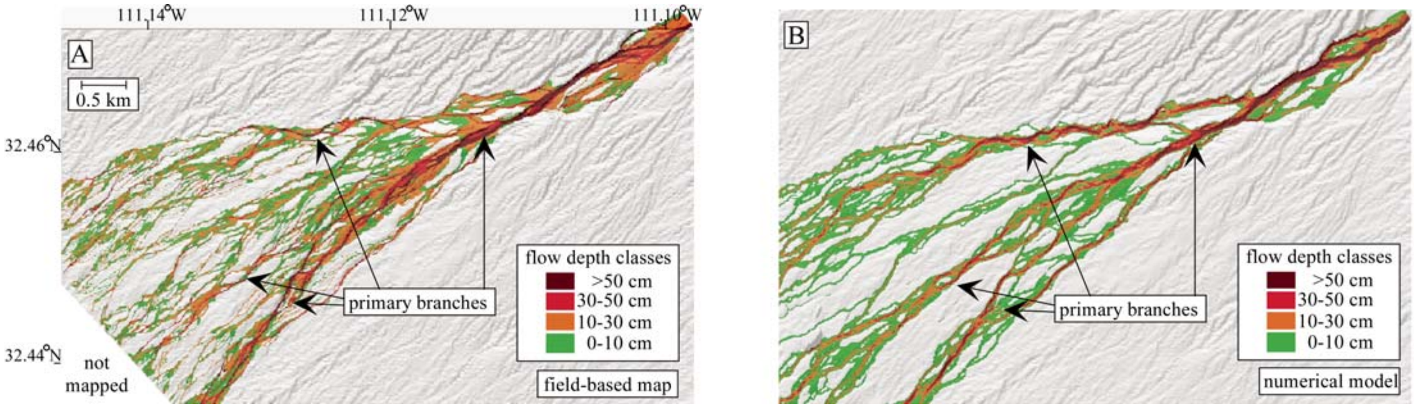

Figure 5. Comparison of (A) field-based inundation map with (B) color map of flow depths predicted from hydrological model for the 27 July 1988 flood in Wild Burro Wash, Tortolita piedmont. The model input included flow depths observed in the field corresponding to a peak discharge of Q = 250 m^3/s. The locations and flow depths of the primary flow branches match each other closely in the two images.

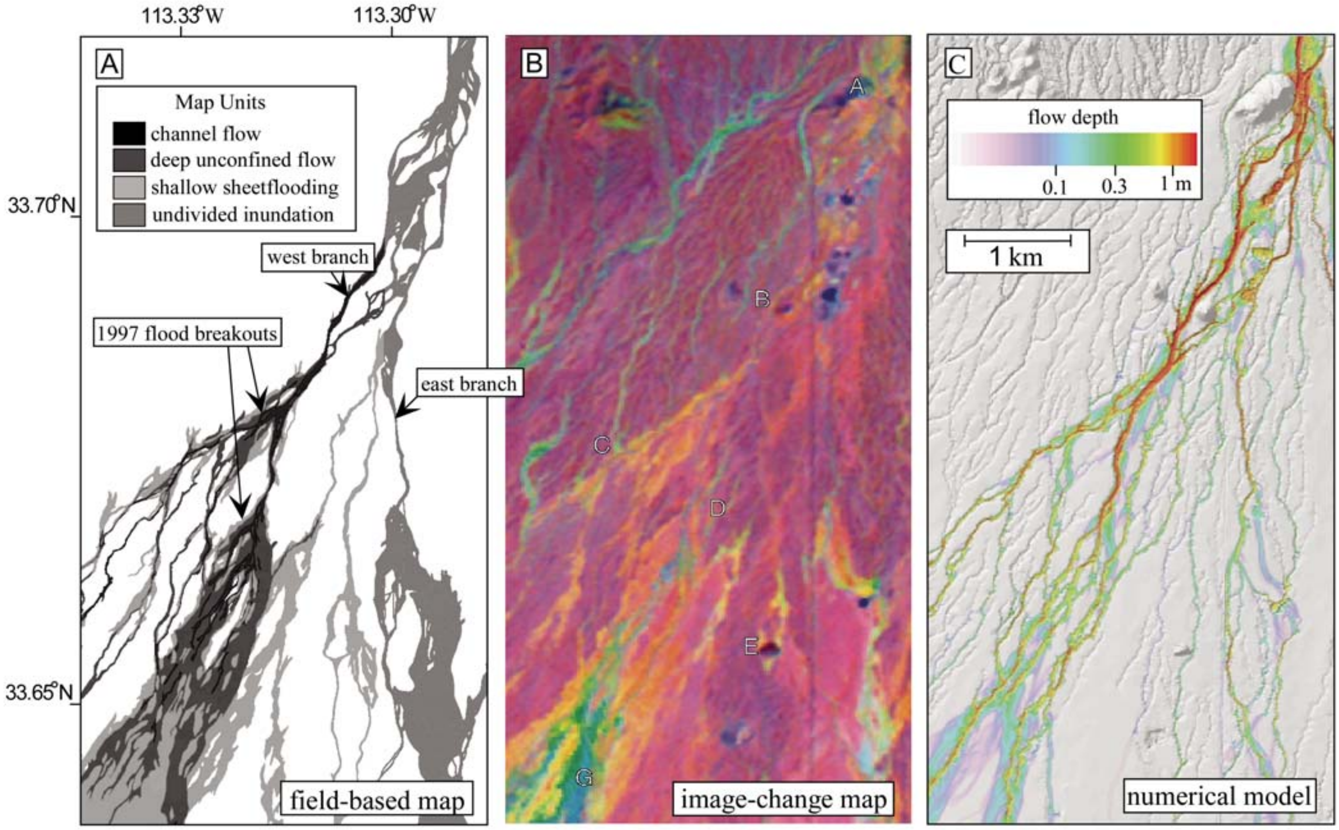

Figure 6. Comparison of (A) field-based inundation map, (B) false-color satellite change-detection map, and (C) color map of flow depth predicted by hydrological model for the 25–26 September 1997 flood in Tiger Wash, Harquahala piedmont. The model input included flow depths at the upstream boundary of the grid corresponding to a peak discharge of Q = 260 m^3/s.

that experienced extensive shallow inundation in the 1997 flood, with relatively fine fresh sediment. Green and cyan colors, which depict areas of increased vegetation cover associated with infiltration of flood waters, were found along some channels, in areas that experienced deep unconfined flow and in areas lower in the distributary system where shallow unconfined flow was more common. Blue areas are extensive in the lower part of the distributary system where flow was shallow and may represent areas where extensive flotsam accumulated.

Numerical Modeling of the Wild Burro and Tiger Wash Floods

The 1988 flood in Wild Burro Wash was modeled using a DEM of the Tortolita piedmont with 5 m resolution (Fig. 1B) and a peak flood discharge of 250 m^3/s. We give the 250 m^3/s discharge as a reference figure for this flood, but what was actually input into the model were flow depths corresponding to the paleoflood stage observed in the field by the AZGS team in 1990 at the upstream corner of the field map.

Overall, the positions and flow depths of the major flow branches match each other closely in the model- (Fig. 5B) and field-based (Fig. 5A) maps. The model predicts a continuous range of flow depths, but we grouped the model depths into the same flow depth classes used in the field map to facilitate comparison. In detail, the model appears to underestimate the extent of lateral overbank flooding in the upper portion of the fan and overestimate the flood extent in the lower portion of the fan. Some of this discrepancy is likely due to the relatively coarse resolution of the input DEM we used. Field mapping in Wild Burro Wash was performed on a 1:200-scale base map and resolves channels that are only a few meters wide. The 5-m-resolution DEM, in contrast, is not capable of resolving flow paths to the level of detail in the field map.

Areas of very shallow flow must be considered carefully when comparing the field- and model-based maps in terms of total inundation. In areas of sheetflooding, the numerical model can predict very shallow flow depths (i.e., <0.1–1 cm) in some areas. These areas should not be included in the flood map for two reasons. First, local slope runoff is likely to dominate the overbank inundation for these very shallow flow depths, and very thin sheets of overbank flow are likely to diminish rapidly by infiltration or bed friction. Second, Manning's equation does not apply to very shallow flows, so there is no physical basis for predicting this class of flow with the numerical model. For these reasons, areas with flow less than 2 cm were removed from the model-based map of Figure 5B.

The 1997 flood on Tiger Wash was reconstructed with the numerical model (Fig. 6C) using a DEM with 3 m resolution (Fig. 4A) and a flood stage corresponding to a peak discharge of 260 m^3/s. We cannot compare these model-predicted flow depths to the other maps in terms of absolute flow depths because the field- and satellite-based maps for Tiger Wash provide only qualitative depth information. Nevertheless, the three maps of Figure 6 are very consistent in terms of the extent of inundation in the western and central portions of the map. The southeastern corner of the study area should not be considered in the comparison because this area received significant incoming flow from a channel that is located off the eastern boundary of the DEM.

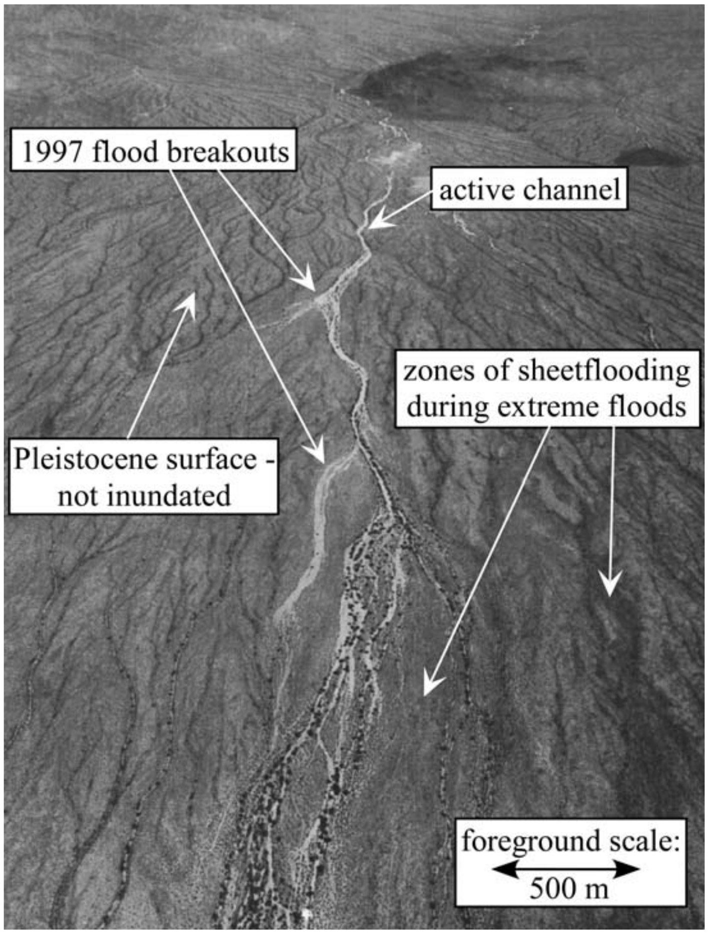

Figure 7. Oblique aerial photograph of western branch of Tiger Wash following the September 1997 flood. Large new channels formed at two breakouts during this flood. Also indicated is a Pleistocene surface that was not inundated in the flood and darker, more heavily vegetated areas that experienced extensive sheetflooding.

PROBABILISTIC FLOOD HAZARD MAPS FOR THE STUDY AREAS AND COMPARISON WITH SURFICIAL GEOLOGIC MAPS

The numerical model was used to predict flow depths for a range of input peak discharges corresponding to the 10 yr, 100 yr, and maximum floods on the Tortolita piedmont (Fig. 8) and Tiger Wash (Fig. 9). For the Tortolita piedmont, we also applied the discharge values of Wild Burro Wash to Cochie and Ruelas Washes in order to estimate the potential flood inundation for the entire piedmont. Cochie and Ruelas Washes have similar drainage areas to Wild Burro (9.8 km^2 for Cochie and 6.0 km^2 for Ruelas), so their peak flood discharges are expected to be comparable.

Flow on the Tortolita piedmont remained confined for even the largest floods (i.e., there is no extensive, laterally continuous sheetflooding), albeit in many channels across the piedmont (Fig. 8). As the input discharge was increased in the model, flood flows became deeper (i.e., more of the map area is colored red, indicating more extensive areas with deep channel flow) and new channels were inundated. Flow in Tiger Wash was also confined for small flows (Fig. 9A), except near the undissected southwestern corner of the area. As peak discharges increased in the Tiger Wash model (Figs. 8B and 8C), the fraction of the study area subjected to unconfined flow grew larger, incorporating areas in the southeastern and northeastern portions of the study area and within a narrow zone along the main channel.

Model predictions of flood inundation for the 10 yr, 100 yr, and maximum floods (Figs. 8 and 9) may be used to create a probabilistic flood hazard map by identifying the input peak discharge required to inundate different surfaces on the piedmont and then assigning

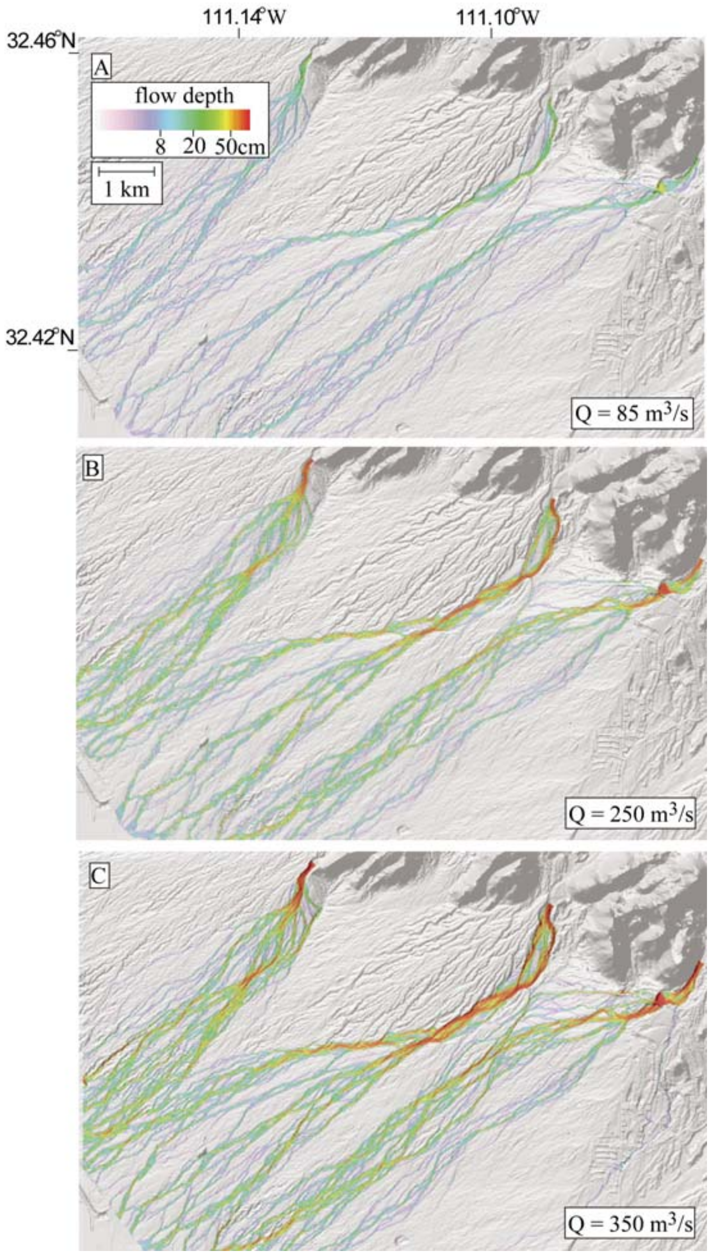

Figure 8. Color maps of model predictions for flow depth on the Tortolita piedmont with input discharges of (A) Q = 85 m^3/s, (B) Q = 250 m^3/s, and (C) Q = 350 m^3/s. These discharges correspond approximately to 10 yr, 100 yr, and maximum floods (Table 1).

the corresponding annual probability to the flooded surface. For example, if a terrace near the active channel is flooded when 100 m^3/s is delivered to the fan, then that terrace is assigned a 0.1 annual probability of flooding because 100 m^3/s corresponds to the 10 yr flood. Inundation of a Pleistocene terrace far from the active channel, however, may require a much greater input discharge, such as 800 m^3/s. The probability of this maximum flood is unclear, but 10^3 is a conservative value. Flood-hazard maps created in this way can be directly compared with surficial geologic and FEMA maps.

The surficial geologic maps for the study areas (Figs. 10B and 11B) were constructed by grouping fan surfaces into approximate age ranges based on factors including local topographic relief, soil development, surface roughness, and vegetation characteristics. Here we describe these maps in more detail in order to specify their surface ages and to compare the associated flood risk with those of the probabilistic maps. Surficial geologic map units for both study areas can be grouped into Holocene and Pleistocene units. The ages of these terraces can be estimated by comparing their relative age indicators to those of terraces of known age (e.g., Gile et al., 1981). The Holocene units were divided into Qyc (active channels), Qy2 (active sheetflood areas and terraces), and Qy1 (young surfaces no longer part of the active system). Qyc and Qy2 refer to active areas that have essentially no soil development. Qy1 areas are older Holocene deposits that have been part of the active depositional system within the past few thousand years but are currently subject to rare flood inundation. Pleistocene units are divided between late (Ql) and middle Pleistocene (Qm) units. Both Pleistocene units have been isolated from active erosion and deposition for at least 10,000 yr and are identified by significant clay accumulation and carbonate development within the soil profile, in addition to characteristic vegetation and topographic shape. In upper fan areas the Pleistocene units are generally higher than adjacent Holocene deposits. In middle and lower fan areas, however, topographic relief between Pleistocene and Holocene units is generally minor.

The probabilistic flood hazard maps (Figs. 10A and 11A) predict areas of active flooding that closely match active areas in the surficial geologic maps (areas mapped as Qyc or Qy2 in Figs. 10B and 11B). In the Tortolita study area, the model-based map predicts a spatially complex pattern of relatively localized flood hazards consistent with the surficial geologic map and inconsistent with the FEMA map. These results provide further evidence that FEMA floodplains delineated with the FAN model do not resolve and generally overpredict the extent of flood-prone areas on the piedmont.

Tiger Wash was one of the first fans in the western United States to be impacted by the revised assessment criteria that allowed geomorphic evidence to be considered in official FEMA flood-hazard assessments. In 2001, FEMA adopted a floodplain map for Tiger Wash (Fig. 11C) that reflects surficial geologic mapping. The resulting map, however, is based on a very conservative interpretation of the surficial geology. Some extensive surfaces that are mapped as part of the 100 yr floodplain (zone A, active or inactive), for example, are Pleistocene-age surfaces. The FEMA map distinguishes between active and inactive fan surfaces, but both units are considered part of the 100 yr floodplain.

Figure 12 compares the results of numerical modeling and surficial geologic mapping with those of the FAN model as a function of distance

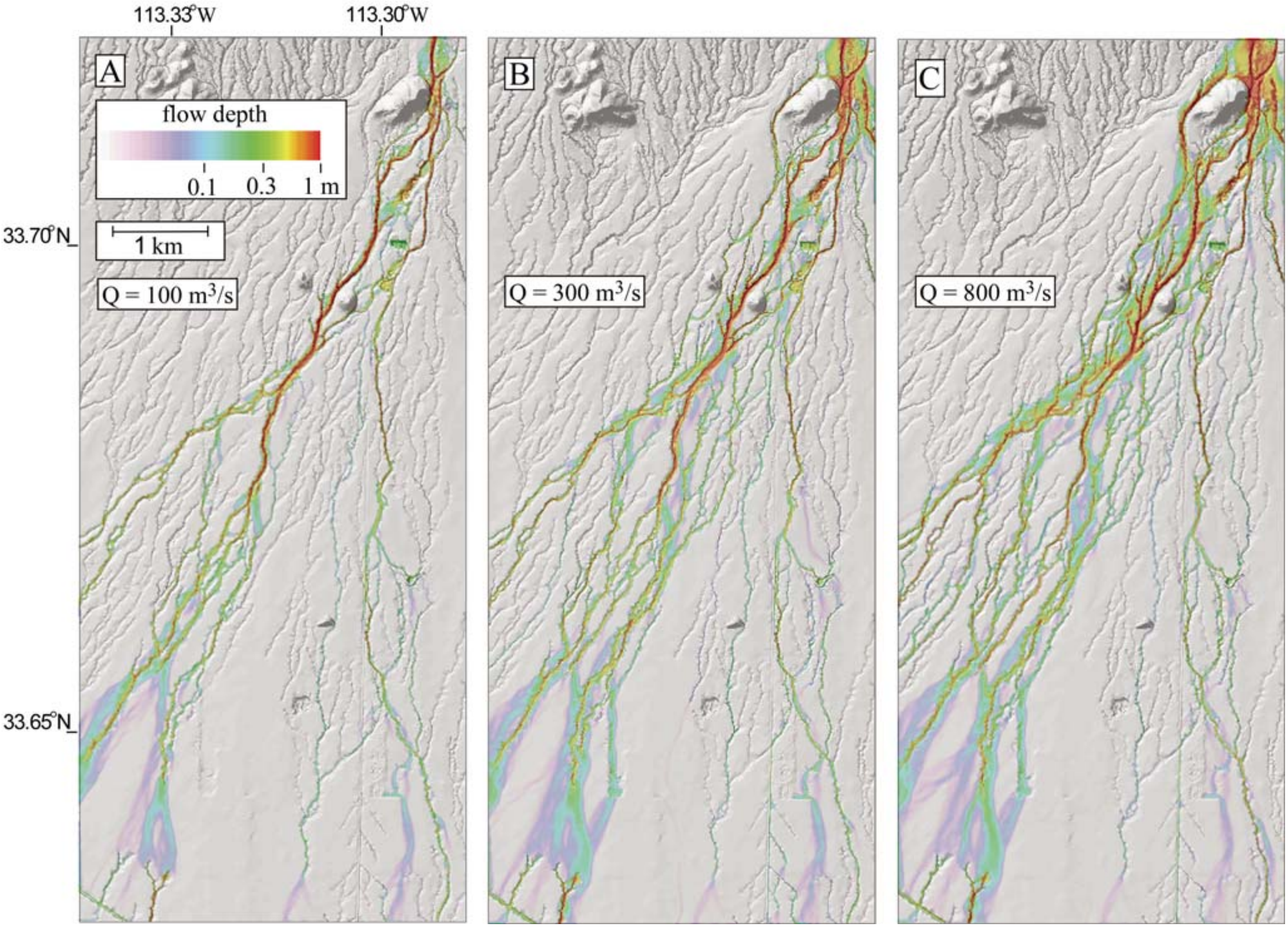

Figure 9. Color maps of model predictions for flow depth on the Harquahala piedmont with input discharges of (A) Q = 100 m^3/s, (B) Q = 300 m^3/s, and (C) Q = 800 m^3/s. These discharges correspond to 10 yr, 100 yr, and maximum floods (Table 1).

from the fan apex. The FAN model predicts a relatively high flood hazard in the proximal area of the fan because flow is deepest at that location. In distal areas, the FAN model predicts extensive inundation but the damage potential is much lower because flow is very shallow (as shown schematically by the depth versus distance curve in Fig. 12B). Although the flow depth is indeed highest near the fan apex, the flood risk there is mitigated by the well-defined and stable character of flooding. Stability is the result of high relief near the fan apex, which serves to confine even extreme flows and to suppress lateral channel migration (Fig. 12A). Numerical modeling (Fig. 12C) indicates that flood risk in distal areas is only marginally lower than in the proximal areas, because typical flood depths do not fall off as quickly with distance as the FAN model predicts. Modeling shows that flow is accommodated across numerous small channels on the fan, rather than spreading out as sheetflow. Surficial geologic mapping provides no information on flow depth, but it corroborates the widespread nature of flood hazards in distal areas while recognizing that Pleistocene deposits have little or no flood risk.

Although the probabilistic flood hazard maps are largely consistent with surficial geologic maps, late Holocene deposits are extensive in some areas (Figs. 9B and 10B) where model-based assessments predict only localized flooding (Figs. 9A and 10A). What is the reason for this discrepancy, and which map is more accurate, the model-based map or the surficial geologic map? The answer is that these maps most likely bracket the true flood hazard because of the difference in time scales between the two maps and because the surficial geologic map includes the effects of erosion and deposition while the model-based map does not. Erosion and deposition during flood events may lead to the lateral migration of active flooding or to the development of channel splays through bank incision. By including the geomorphic evolution resulting from many flood events that have occurred over thousands of years, the surficial geologic map most likely overestimates the flooding that would occur during a single flood. However, by neglecting erosion and deposition entirely, the model-based assessment most likely underestimates flood hazards in areas where channel changes are likely to occur during a flood. Erosion and deposition can be included in numerical models by using a convection-diffusion model of sediment transport (e.g., Ariathurai and Krone, 1976; Letter et al., 2000). Some 2D hydrodynamic models currently have this capability, and these models could be used to further refine flood hazards.

SUMMARY AND CONCLUSIONS

Surficial geologic mapping has demonstrated that for many areas the FAN model predicts flood inundation where it cannot occur. Surficial geologic mapping provides a powerful alternative to the FAN model because it uses the actual long-term record of flood inundation to predict where flooding could occur in the future, including the

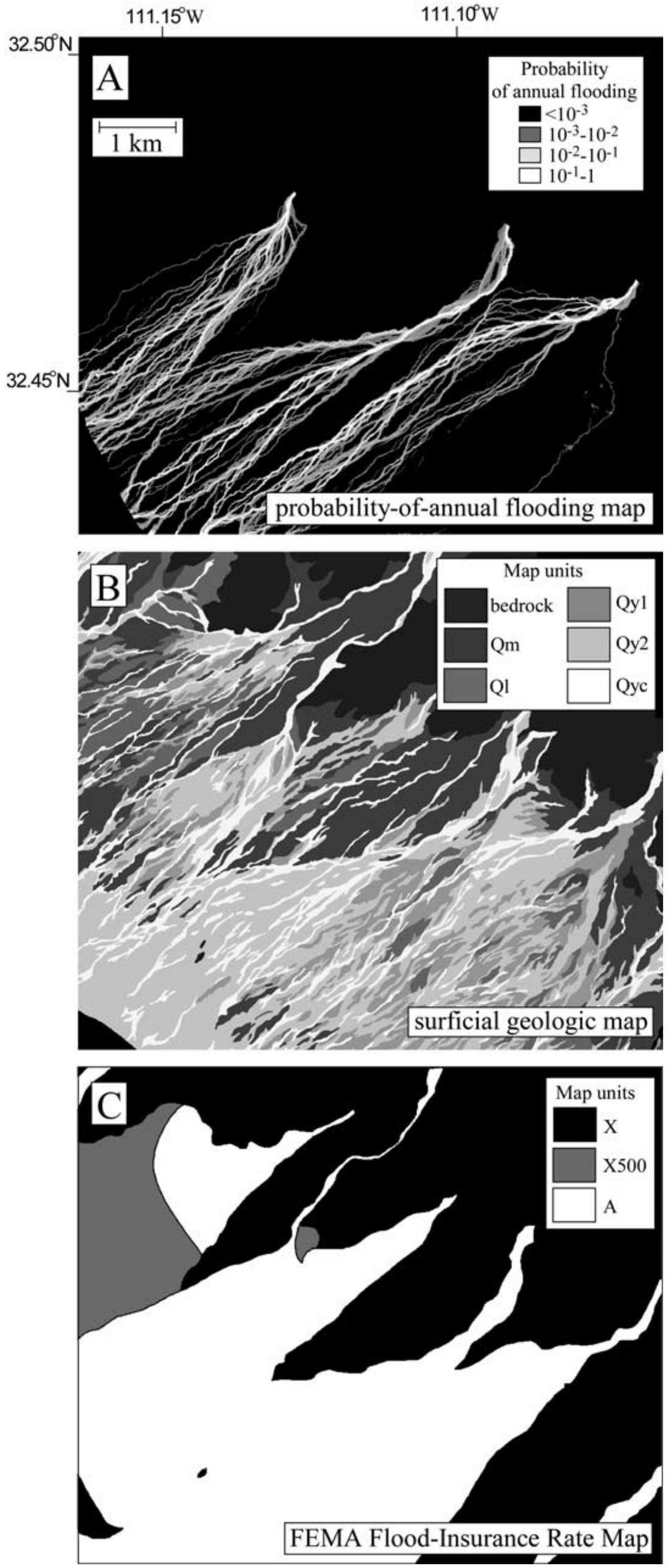

Figure 10. (A) Model-based probability-of-annual-flooding map, (B) surficial geologic map (after Demsey et al., 1993), and (C) Federal Emergency Management Agency (FEMA) Flood-Insurance Rate Map for the Tortolita piedmont (after FEMA, 1999).

effects of erosion and deposition. Surficial geologic mapping may be overly conservative, however, because the long-term record of flooding includes flood inundation associated with many large floods over thousands of years, not just a single flood that could occur in the near future.

Geomorphic mapping of the inundation extents of recent extreme floods provides direct observations of flood behavior for a specific event, including processes of erosion and deposition, and it constrains the flow regimes in different topographic settings on the fan. This method is also limited, however, because it is time intensive and does not constrain the behavior of floods that are much larger or much smaller than recent large floods. Satellite-image change detection delivers some of the same information provided by geomorphic mapping of individual floods, but has the advantage that it can be applied over a large area in a relatively short period of time. Nevertheless, the satellite method still does not predict flood inundation for a specified discharge (i.e., the standard regulatory flood).

Numerical modeling enables direct observations of recent flood behavior based on field- and satellite-based methods to be linked with predictions of flood behavior for specific discharges. To make this linkage, numerical models must be validated against direct observations of recent floods, providing a basis for using the model to predict the flood inundation corresponding to large floods that have not occurred recently, including the 100 yr and maximum floods. Geomorphic mapping, satellite-image change detection, and modeling therefore provide a powerful composite methodology for flood hazard assessments. Geomorphic mapping and satellite-image change detection are important because they include the effects of erosion and deposition, while most numerical models do not. Each method provides assessments over time scales that overlap with the predictions of other methods, providing ample opportunities for cross checking of results. Numerical model results, for example, may be compared with satellite-image change detection over short time scales and with surficial geologic maps over long time scales.

ACKNOWLEDGMENTS

We wish to thank the Flood Control District of Maricopa County for providing the high-resolution DEM data for Tiger Wash and the Pima Association of Governments for providing DEM data for the Tortolita piedmont. The modeling aspect of this work was supported by NSF grant EAR-0309518 to Pelletier. Field investigations of the Tortolita piedmont were supported by the Pima County Flood Control District and the Arizona Geological Survey; field investigations of Tiger Wash were supported by the Flood Control District of Maricopa County and the Arizona Geological Survey. We wish to thank Paul Bierman, Ramon Arrowsmith, and Lisa Ely for very helpful reviews.

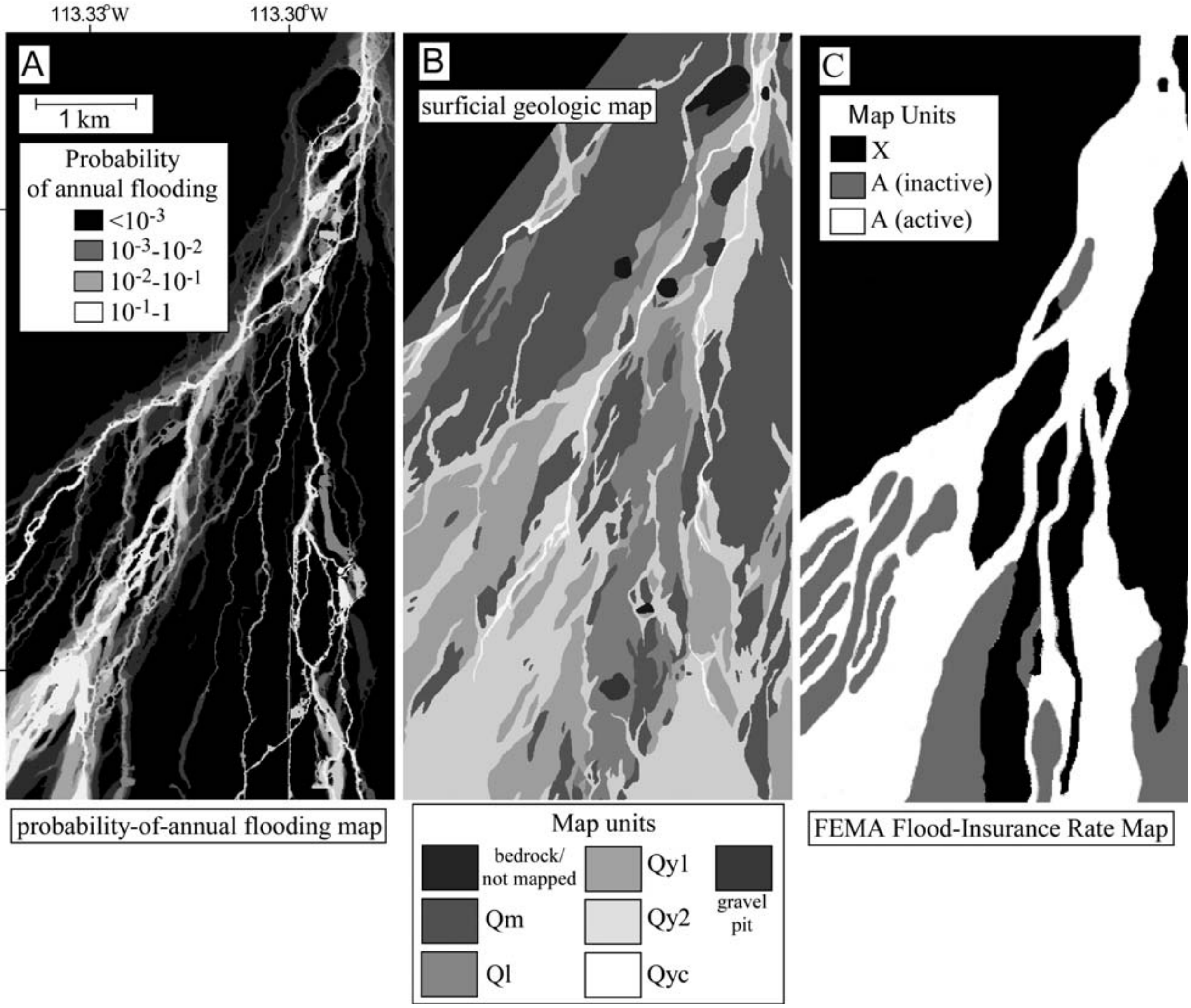

Figure 11. (A) Model-based probability-of-annual-flooding map, (B) surficial geologic map (after Klawon and Pearthree, 2000), and (C) FEMA Flood Insurance Rate Map (after FEMA, 2001) for the Tiger Wash portion of the Harquahala piedmont.

REFERENCES CITED

Ariathurai, R., and Krone, R.B., 1976, Finite element model for cohesive sediment transport: Journal of the Hydraulics Division, American Society of Civil Engineers, v. 102, p. 323–338.

Bates, P.D., and De Roo, A.P.J., 2000, A simple raster-based model for flood inundation simulation: Journal of Hydrology, v. 236, p. 54–77.

Bull, W.B., 1991, Geomorphic Responses to Climatic Change: New York, Oxford University Press, 326 p.

Cain, J.M., and Beatty, M.T., 1968, The use of soil maps in the delineation of flood plains: Water Resources Research, v. 4, p. 173–182.

CHM2Hill, 1992, Alluvial fan data collection and monitoring study: A report to the Flood Control District of Maricopa County: Phoenix, Arizona, CHM2Hill, 204 p., 2 pl.

Dawdy, D.R., 1979, Flood-frequency estimates on alluvial fans: Journal of the Hydraulics Division, American Society of Civil Engineers, v. 105, p. 1407–1413.

Demsey, K.A., House, P.K., and Pearthree, P.A., 1993, Detailed surficial geologic map of the southern piedmont of the Tortolita Mountains, Pima County, southern Arizona: Arizona Geological Survey Open-File Report 93-14, scale 1:24,000, 8 p., 1 sheet.

Enzel, Y., Ely, L.L., House, P.K., Baker, V.R., and Webb, R.H., 1993, Paleoflood evidence for a natural upper bound to flood magnitudes in the Colorado River Basin: Water Resources Research, v. 29, p. 2287–2297.

Eychaner, J.H., 1984, Estimation of the magnitude and frequency of floods in Pima County, Arizona, with comparisons of alternative methods: U.S. Geological Survey Water Resources Investigations Report 84-4142, 69 p.

Federal Emergency Management Agency (FEMA), 1990, FAN: An Alluvial Fan Flooding Computer Program, User's Manual and Program Disk: Washington, D.C., Federal Emergency Management Agency.

Federal Emergency Management Agency (FEMA), 1999, Flood Insurance Rate Maps (FIRMs), Pima County, unincorporated areas.

Federal Emergency Management Agency (FEMA), 2000, Guidelines for determining flood hazards on alluvial fans: http://www.fema.gov/fhm/dl_alfan.shtm, 23 p.

Federal Emergency Management Agency (FEMA), 2001, Flood Insurance Rate Maps (FIRMs), Maricopa County, unincorporated areas.

Field, J.J., 2001, Channel avulsion on alluvial fans in southern Arizona: Geomorphology, v. 37, p. 93–104.

Field, J.J., and Pearthree, P.A., 1991a, Surficial geology around the White Tank Mountains, central Arizona: Arizona Geological Survey Open-File Report 91-8, scale 1:24,000, 7 p., 9 sheets.

Field, J.J., and Pearthree, P.A., 1991b, Geologic mapping of flood hazards in Arizona: An example from the White Tank Mountains area, Maricopa County: Arizona Geological Survey Open-File Report 91-10, scale 1:24,000, 16 p., 4 sheets.

Flood Control District of Maricopa County (FCDMC), 2001, Digital DTM data: http://www.fcd.maricopa.gov.

Flood Control District of Maricopa County (FCDMC), 2003, Alert Flood Warning System, stream gage data: http://fcd.maricopa.gov/alert/alert.htm.

French, R.H., 1987, Hydraulic Processes on Alluvial Fans: Amsterdam, Elsevier, 244 p.

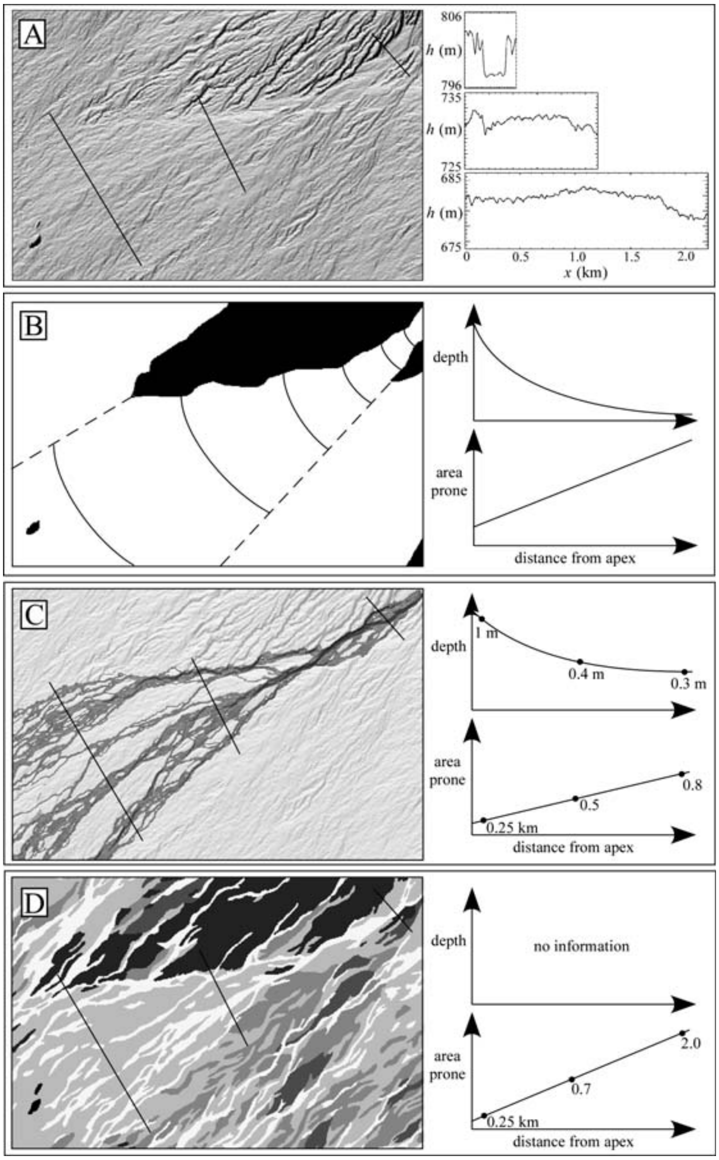

Figure 12. (A) Fan topography, illustrating decrease in along-strike relief with distance from fan apex. Comparison of (B) FAN model, (C) numerical model, and (D) surficial geologic predictions in terms of flow depth and flood-prone area.

French, R.H., Fuller, J.E., and Waters, S., 1993, Alluvial fan: Proposed new process-oriented definitions for arid southwest: Journal of Water Resources Planning and Management, American Society of Civil Engineers, v. 119, p. 588–598.

Fuller, J.E., 1990, Misapplication of the FEMA alluvial fan model: A case history, *in* French, R.H., ed., Hydraulics and Hydrology of Arid Lands: New York, American Society of Civil Engineers, p. 367–377.

Galland, J.C., Goutal, N., and Hervouet, J.-M., 1991, TELEMAC—A new numerical model for solving shallow-water equations: Advances in Water Resources, v. 14, p. 138–148.

Gile, L.H., Hawley, J.W., and Grossman, R.B., 1981, Soils and geomorphology in the Basin and Range area of southern New Mexico—Guidebook to the Desert Project: New Mexico Bureau of Mines and Mineral Resources Memoir 39, 222 p.

Grant, G., 1997, Critical flow constrains flow hydraulics in mobile-bed streams—A new hypothesis: Water Resources Research, v. 33, p. 349–358.

Hjalmarson, H.W., 1994, Potential flood hazards and hydraulic characteristics of distributary-flow areas in Maricopa County, Arizona: U.S. Geological Survey Water Resources Investigations Report 93-4169, 56 p.

Hooke, R.L., 1972, Geomorphic evidence for late Wisconsin and Holocene tectonic deformation, Death Valley, California: Geological Society of America Bulletin, v. 83, p. 2073–2098.

Horritt, M.S., and Bates, P.D., 2001a, Effects of spatial resolution on a raster based model of flood flow: Journal of Hydrology, v. 253, p. 239–249.

Horritt, M.S., and Bates, P.D., 2001b, Predicting floodplain inundation: Raster-based modeling versus the finite-element approach: Hydrological Processes, v. 15, p. 825–842.

Horritt, M.S., and Bates, P.D., 2002, Evaluation of 1D and 2D numerical models for predicting river flood inundation: Journal of Hydrology, v. 268, p. 87–99.

House, P.K., 1991, Paleoflood hydrology of the principal canyons of the southern Tortolita Mountains, southeastern Arizona: Arizona Geological Survey Open-File Report 91-6, 31 p.

House, P.K., 2003, Geologic Mapping—An essential but frequently ignored component of flood hazard assessment on desert piedmonts: Geological Society of America Abstracts with Programs, v. 34, p. 72.

House, P.K., Pearthree, P.A., and Vincent, K.R., 1991, Flow patterns, flow hydraulics, and flood-hazard implications of a recent extreme alluvial-fan flood in southern Arizona: Geological Society of America Abstracts with Programs, v. 23, p. 121.

House, P.K., Pearthree, P.A., and Vincent, K.R., 1992, Geological insights into deficiencies in federal procedures for flood hazard assessment on alluvial fans: Geological Society of America Abstracts with Programs, v. 24, p. 284.

J.E. Fuller Hydrology, and Geomorphology, 2000, Inundation mapping of the September 1997 flood, surficial geologic mapping, and evaluation of the piedmont flood hazard assessment manual for portions of the Tiger Wash piedmont: Report to the Flood Control District of Maricopa County, Contract 98-48.

King, I.P., and Norton, W.R., 1978, Recent application of RMA's finite element models for two-dimensional hydrodynamics and water quality, *in* Proceedings of the 2nd International Conference on Finite Elements in Water Resources: London, Pentec Press, p. 81–99.

Klawon, J.E., and Pearthree, P.A., 2000, Field guide to a dynamic distributary drainage system: Tiger Wash, western Arizona: Arizona Geological Survey Open-File Report 00-1, scale 1:70,000, 34 p., 1 sheet.

Letter, J.V., Donnell, B.P., McAnally, W.H., and Thomas, W.A., 2000, A User's Manual for SED2D WES Version 4.5: Vicksburg, Mississippi, U.S. Army Corps of Engineers Waterways Experiment Station, 174 p.

Mayer, L., 2000, Satellite remote sensing of flood related landscape change resulting from hurricanes in Baja California and the southwestern United States, *in* Hassan, M.A., et al., eds., The Hydrology-Geomorphology Interface: Rainfall, Floods, Sedimentation, Land Use: International Association of Hydrological Sciences Publication 261, p. 201–214.

Mayer, L., 2002, Landsat-based flood detection in the Jackrabbit Wash area, Maricopa County, Arizona, *in* Youberg, A., ed., A compilation of geomorphologic and hydrological reports on the Jackrabbit Wash flood, October, 2000, Maricopa County, Arizona: Arizona Geological Survey Open-File Report 02-06, 98 p.

Mayer, L., and Pearthree, P.A., 2002, Mapping flood inundation in southwestern Arizona using Landsat TM data: A method for rapid regional flood assessment following large storms, *in* House, P.K., et al., eds., Paleoflood Monograph: Washington, D.C., American Geophysical Union, p. 61–75.

McFadden, L.D., Ritter, J.B., and Wells, S.G., 1989, Use of multi-parameter relative-age estimates for age estimation and correlation of alluvial fan surfaces on a desert piedmont, Eastern Mojave Desert, California: Quaternary Research, v. 32, p. 276–290.

Miyamoto, H., Baker, V.R., and Komatsu, G., 2003, Semi-three-dimensional computer simulations of large-scale cataclysmic flooding: A model and parameter sensitivities: Lunar and Planetary Science Conference Abstracts, v. 34, p. 1724.

National Research Council, 1996, Alluvial Fan Flooding: Washington D.C., National Academy Press, 172 p.

O'Brien, J.S., Julien, P.Y., and Fullerton, W.T., 1993, Two-dimensional water flood and mudflow simulation: Journal of Hydraulic Engineering, American Society of Civil Engineers, v. 119, p. 244–259.

Pearthree, P.A., 1991, Geomorphic insights into flood hazards in piedmont areas in Arizona: Arizona Geology, v. 21, p. 1–5.

Pearthree, P.A., Demsey, K.A., Onken, J., Vincent, K.R., and House, P.K., 1992, Geomorphic assessment of flood-prone areas on the southern piedmont of the Tortolita Mountains, Pima County, Arizona: Arizona Geological

Survey Open-File Report 91-11, scale 1:12,000 and 1:24,000, 31 p. and 4 sheets.

Pearthree, P.A., House, P.K., and Vincent, K.R., 2000, Geomorphologic assessment of alluvial fan flood hazards in southern and central Arizona, *in* Floodplain Management in the Desert: Arid Regions Floodplain Management 8th Biennial Conference: Las Vegas, Nevada, Association of State Floodplain Managers, p. 82–91.

Pearthree, P.A., Klawon, J.E., and Lehman, T.W., 2004, Geomorphology and hydrology of an alluvial fan flood on Tiger Wash, Maricopa and La Paz Counties, west-central Arizona: Arizona Geological Survey Open-File Report 04-02, 40 p.

Pima Association of Governments (PAG), 2000, Digital DTM data: http://www.pagnet.org/RDC.

Pope, G.L., Rigas, P.D., and Smith, C.F., 1998, Statistical summaries of streamflow data and characteristics of drainage basins for selected streamflow-gaging stations in Arizona through water year 1996: U.S. Geological Survey Water Resources Investigations Report 98-4225, 907 p.

Press, W.H., Flannery, B.P., Teukolsky, S.A., and Vetterling, W.T., 1992, Numerical Recipes in C: The Art of Scientific Computing, Second Edition: New York, Cambridge University Press, 994 p.

Reheis, M.C., Slate, J.L., Throckmorton, C.K., McGeehin, J.P., Sarna-Wojcicki, A.M., and Dengler, L., 1996, Late-Quaternary sedimentation on the Leidy Creek fan, Nevada-California: Geomorphic responses to climate change: Basin Research, v. 8, p. 279–299.

Ritter, D.F., 1967, Terrace development along the front of the Beartooth Mountains, southern Montana: Geological Society of America Bulletin, v. 78, p. 467–484.

Rockwell, T.K., Keller, E.A., and Johnson, D.L., 1985, Tectonic geomorphology of alluvial fans and mountain fronts near Ventura, California, *in* Morisawa, M., and Hack, J.T., eds., Tectonic geomorphology: Binghamton Symposia in Geomorphology International Series, v. 15, p. 183–207.

Schumm, S.A., and Parker, R.S., 1973, Implications of complex response of drainage systems for Quaternary alluvial stratigraphy: Nature, v. 243, p. 99–100.

U.S. Army Corps of Engineers Waterways Experiment Station, 2001, User's Guide to RMA2-WES Version 4.5: Vicksburg, Mississippi, 76 p.

Vincent, K.R., and Smith, J.D., 2001, Hydraulic processes in channels of water-lain alluvial piedmonts in arid lands: Eos (Transactions, American Geophysical Union), v. 82, p. F387.

Vincent, K.R., Pearthree, P.A., House, P.K., and Demsey, K.A., 2004, Inundation mapping and hydraulic reconstructions of an extreme alluvial fan flood, Wild Burro Wash, Pima County, southern Arizona: Arizona Geological Survey Open File Report 04-04, 45 p., 1 plate and GIS data on disk.

Youberg, A., and Pearthree, P.A., 2002, Geomorphic assessment of the October 2000 flood on Jacrabbit Wash, *in* Youberg, A., ed., A compilation of geomorphologic and hydrological reports on the Jackrabbit Wash flood, October, 2000, Maricopa County, Arizona: Arizona Geological Survey Open-File Report 02-06, 98 p.

Manuscript Received by the Society 14 December 2003
Revised Manuscript Received 16 November 2004
Manuscript Accepted 3 January 2005

Printed in the USA